Journal of Hydrology 581 (2020) 124456

Contents lists available at ScienceDirect

Journal of Hydrology

journal homepage: www.elsevier.com/locate/jhydrol

Research papers

Evaluation and integration of the top-down and bottom-up satellite precipitation products over mainland China

Ling Zhang[a,*], Xin Li[b,c], Yanping Cao[d], Zhuotong Nan[e], Weizhen Wang[a], Yingchun Ge[a], Penglong Wang[a], Wenjun Yu[f]

[a] Key Laboratory of Remote Sensing of Gansu Province, Northwest Institute of Eco-Environment and Resources, Chinese Academy of Sciences, Lanzhou 730000, China
[b] Institute of Tibetan Plateau Research, Chinese Academy of Sciences, Beijing 100101, China
[c] CAS Center for Excellence in Tibetan Plateau Earth Sciences, Beijing 100101, China
[d] The College of Environment and Planning of Henan University, Kaifeng 475004, Henan, China
[e] Ministry of Education Key Laboratory of Virtual Geographic Environment, Nanjing Normal University, Nanjing 210023, China
[f] College of Hydrometeorology, Nanjing University of Information Science &Technology, 210023 Nanjing, China

ARTICLE INFO

This manuscript was handled by Emmanouil Anagnostou, Editor-in-Chief, with the assistance of Yiwen Mei, Associate Editor

Keywords:
Satellite precipitation products
IMERG
SM2RAIN-ASCAT
Performance evaluation
Data integration
Mainland China

ABSTRACT

The satellite precipitation products (SPPs) obtained from the satellite soil moisture data through a bottom-up approach (i.e., the SM2RAIN algorithm) have been developed and released in recent years. However, the assessments and the integration of them with the conventional top-down SPPs remain absent over China. This study evaluated and integrated, for the first time, the bottom-up SM2RAIN-ASCAT (SM2RASC) product and the top-down Integrated Multi-satellite Retrievals for Global Precipitation Measurement (IMERG) Early Run product over mainland China. The evaluations were conducted at multiple temporal scales using both the continuous and categorical metrics; and the integration was implemented through a nudging scheme. Results indicate that IMERG outperforms SM2RASC in terms of CC at the daily scale. Meanwhile, it achieves a better performance than SM2RASC in detecting precipitation events. However, interestingly, IMERG performs worse than SM2RASC in terms of CC and NRMSE at the monthly scale. Both IMERG and SM2RASC show noticeable seasonal variability regarding the performance, with better qualities in the wet seasons than in the dry seasons. Spatially, IMERG performs better in the humid subregions than in the semi-arid subregions in terms of CC, while SM2RASC performs better in the semi-arid region than in the other subregions. Both of them perform relatively worse in the complex mountainous subregion (i.e. the Qinghai-Tibetan Plateau) and the arid subregion. The performances of the SPPs are closely correlated to the elevations and precipitation magnitudes. The correlations and their significances, however, vary between IMERG and SM2RASC, and between different time scales and different evaluation metrics. The integrated product could increase the median CC by up to 25.86% (or 7.23%), and reduce the median NRMSE by up to 14.72% (or 24.62%), at the daily (or monthly) scale in the validation period (i.e., 2012–2017), compared to the parent products. This study demonstrated the overall good performance of SM2RASC over mainland China, particularly in the semi-arid region, and meanwhile, highlighted the strong benefits of integrating the bottom-up and top-down SPPs.

1. Introduction

Precipitation typically shows strong spatio-temporal variability (Bárdossy and Pegram, 2013), and is one of the major components in the hydrological cycle and land–atmosphere interactions (Brocca et al., 2016; Huang et al., 2016). Accurate and reliable information of precipitation are therefore critical for various fields in geoscience such as hydrological and ecological modeling (Lima et al., 2018), water resource managements (Supit et al., 2012), climate analyses (Chen et al., 2019), flood and drought monitoring (Hui-Mean et al., 2018; Yuan et al., 2019; Zhong et al., 2019), and landslide modeling and forecast (Brunetti et al., 2018). The rain gauge network is the conventional method used to measure precipitation at the point scale. Nevertheless, the density and spatial patterns of the rain gauge networks diverge significantly across the globe (Kucera et al., 2012), without or with scarce gauge stations over the remote mountainous and oceanic regions, and the developing countries (Rozante et al., 2018).

The satellite precipitation products (SPPs) evolve rapidly over the

* Corresponding author.
E-mail address: zhanglingky@lzb.ac.cn (L. Zhang).

https://doi.org/10.1016/j.jhydrol.2019.124456
Received 18 August 2019; Received in revised form 27 October 2019; Accepted 10 December 2019
Available online 12 December 2019
0022-1694/ © 2019 Elsevier B.V. All rights reserved.

last few decades, and offer an alternative and promising approach for obtaining spatially distributed precipitation with relatively high spatiotemporal resolutions (Huffman et al., 2007; Xu et al., 2017). The primarily advantages of the SPPs over the rain gauge network lie in that they could estimate precipitation over the ungauged areas, and meanwhile, have higher capabilities in capturing spatial variability of precipitation at large scales such as the large river basin, continent and globe. Nevertheless, because of the indirect retrieval of the precipitation, the SPPs are inherently subjected to some drawbacks arising from the deficiency of the sensors, retrieval algorithms and observing frequency (Ciabatta et al., 2015; Tian et al., 2015; Ebrahimi et al., 2017). It is therefore necessary and essential to perform an evaluation of the SPPs before their applications.

Currently, there are a series of SPPs available to the public such as the Climate Precipitation Center morphing method (CMORPH) (Joyce et al., 2004), Precipitation Estimation from Remotely Sensed Information using Artificial Neural Networks (PERSIANN) (Hsu et al., 1997; Sorooshian et al., 2000) and Tropical Rainfall Measuring Mission (TRMM) multi-satellite precipitation analysis (TMPA) products (Huffman et al., 2007), among which TMPA is perhaps the most widely used one, and brings considerable science contributions and societal benefits. Nevertheless, the TMPA product has a planned end date of December 31, 2019 (https://pmm.nasa.gov/TRMM). Building upon the success of the TRMM, the Global Precipitation Measurement (GPM) mission, initiated by NASA and the Japan Aerospace Exploration Agency (JAXA), provides the next-generation global precipitation estimates at fine spatio-temporal resolutions ($0.1^\circ \times 0.1^\circ$ and 30-min). Hence, the Integrated Multi-Satellite Retrievals for GPM (IMERG) (Huffman et al., 2014), as the successor to TMPA, is now the recommended multi-satellite dataset to use for various purposes. Like TMPA, the precipitation estimates of the newly released IMERG product are based on the conventional and top-down approach through the inversion of the atmospheric signals emitted or scattered by hydrometeors (Kucera et al., 2012; Brocca et al., 2016). In recent years, the IMERG product has been extensively evaluated against the ground-based observations in different regions around the world (e.g. Tang et al., 2016; Dezfuli et al., 2017; Xu et al., 2017; Chiaravalloti et al., 2018; Omranian et al., 2018; Palomino-Ángel et al., 2019). It is generally reported that IMERG could reasonably capture the spatio-temporal variability of precipitation, and outperform its predecessor (i.e., TMPA).

In addition to the conventional top-down SPPs, the bottom-up ones such as SM2RAIN-CCI (Ciabatta et al., 2018) and SM2RAIN-ASCAT (Brocca et al., 2019) have been developed and released to the public in recent years. The precipitation retrievals in these SPPs are based on the SM2RAIN algorithm proposed by Brocca et al. (2013), an innovative and bottom-up approach that uses satellite soil moisture observations to indirectly estimate rainfall over land. The assumption behind this approach is very simple, i.e., an increase of soil moisture can be closely related to rainfall events (Brocca et al., 2016). The bottom-up SPPs have been evaluated at both regional and global scales. Brocca et al. (2014) obtained three new global precipitation products from the satellite soil moisture data including SMOS, ASCAT and AMSR, and found that they could have better performance than the TRMM-3B42RT product. Prakash (2019) have conducted the assessment of SM2RAIN-CCI across India, and concluded that it underestimate precipitation considerably as compared to the gauge-based observations. Paredes-Trejo et al. (2019) have evaluated the SM2RAIN-ASCAT, SM2RAIN-CCI and TMPA products over Brazil, and reported that the former performs better than the latter two products. Rahman et al. (2019b) assessed SM2RAIN-CCI and SM2RAIN-ASCAT over Pakistan, and found that both of them perform worse than TMPA across all climate regions. At present, however, the evaluation of the bottom-up SPPs over China is still absent, which is an important motivation behind this study.

The top-down and bottom-up SPPs have both pros and cons in capturing different aspects of the precipitation (Brocca et al., 2016). For example, the former one has the limitations in retrieving light rainfall, while the later suffers from the problems of estimating rainfall when the soil is close to saturation (Ciabatta et al., 2017). Hence, the integration of them is highly desirable to increase the accuracy of rainfall estimates. Ciabatta et al. (2015) merged SM2RIAN-ASCAT and the real-time (3B42-RT) TMPA product over Italy. Brocca et al. (2016) integrated SM2RAIN-SMOS and TMPA 3B42RT over Australia. Tarpanelli et al. (2017) implemented a two-phase integration of three SM2RAIN-derived rainfall products and the IMERG product in India and Italy. Chiaravalloti et al. (2018) combined the IMERG product with SM2RIAN-ASCAT over complex terrain in southern Italy. These studies reported various degrees of performance improvements for the merged product. Nevertheless, to our best knowledge, the integration of bottom-up products with the bottom-up ones has not been implemented before over China, which is the other important motivation of this study.

To fill the gaps above, this research is carried out with two paramount objectives. One is to evaluate the SM2RAIN-ASCAT and IMERG products by using the ground-based observations from 701 meteorological stations across mainland China. The other is to integrate the two SPPs and investigate the potential performance improvements for the merged product. The evaluations were conducted for IMERG and SM2RAIN-ASCAT as well as the integrated product at multiple temporal scales by using both the continuous and categorical metrics. The seasonal and spatial variabilities of the performances of the SPPs, and the performance dependence on the elevations and precipitation magnitudes were further investigated in this study.

2. Study area and data

2.1. Study area

This study was carried out over mainland China, which locates between about 15°-50°N and 65°-135°E, and covers an area of about 9.6 million km^2 (Fig. 1). It is characterized by the large variability of elevations, ranging from 152 m below the sea level in east China to 7,528 m above the sea level on the Qinghai-Tibetan Plateau (QTP). As shown in Fig. 1, mainland China could be subdivided into eight subregions (Chen et al., 2013; Chen and Li, 2016), according to the precipitation distribution, mountain ranges and elevations. They are the Xinjiang region (XJ), the Qinghai-Tibetan Plateau (QTP), the middle- and downstream Yangtze River Basin (YZ), the southwest Yungui Plateau (YGP), Northwest China (NWC), Northeast China (NEC), North China (NC), and Southeast China (SEC). The arid and semi-arid subregions (i.e., XJ and NEC) are dominated by a temperate continental climate, with scarce precipitation and intensive evaporation. The humid subregions YZ, YGP and SEC, on the contrary, are controlled by tropical and sub-tropical climates with abundant precipitation (Wang et al., 2019b). The subregions NEC and NC are mainly influenced by the temperate monsoon climate of medium latitudes with hot and wet summer, and cold and dry winter. The QTP is characterized by very complex terrains with an average elevation higher than 4,000 m, and has a distinct plateau climate features in strong radiation, low temperature and highly variable precipitation patterns (Yu et al., 2015).

2.2. Data

2.2.1. Top-down satellite precipitation product

The level-3 product of GPM (i.e., IMERG) was generated through the intercalibration, interpolation and integration of “all” satellite microwave precipitation estimates, precipitation gauge analyses, microwave-calibrated infrared (IR) satellite estimates, and other precipitation estimators at fine spatio-temporal scales for the TRMM and GPM eras (Huffman et al., 2014). Compared to its predecessor TMPA, the main advantage of IMERG is the extended capability to measure light rain (< 0.5 mm hr-1) and solid precipitation. The IMERG product currently

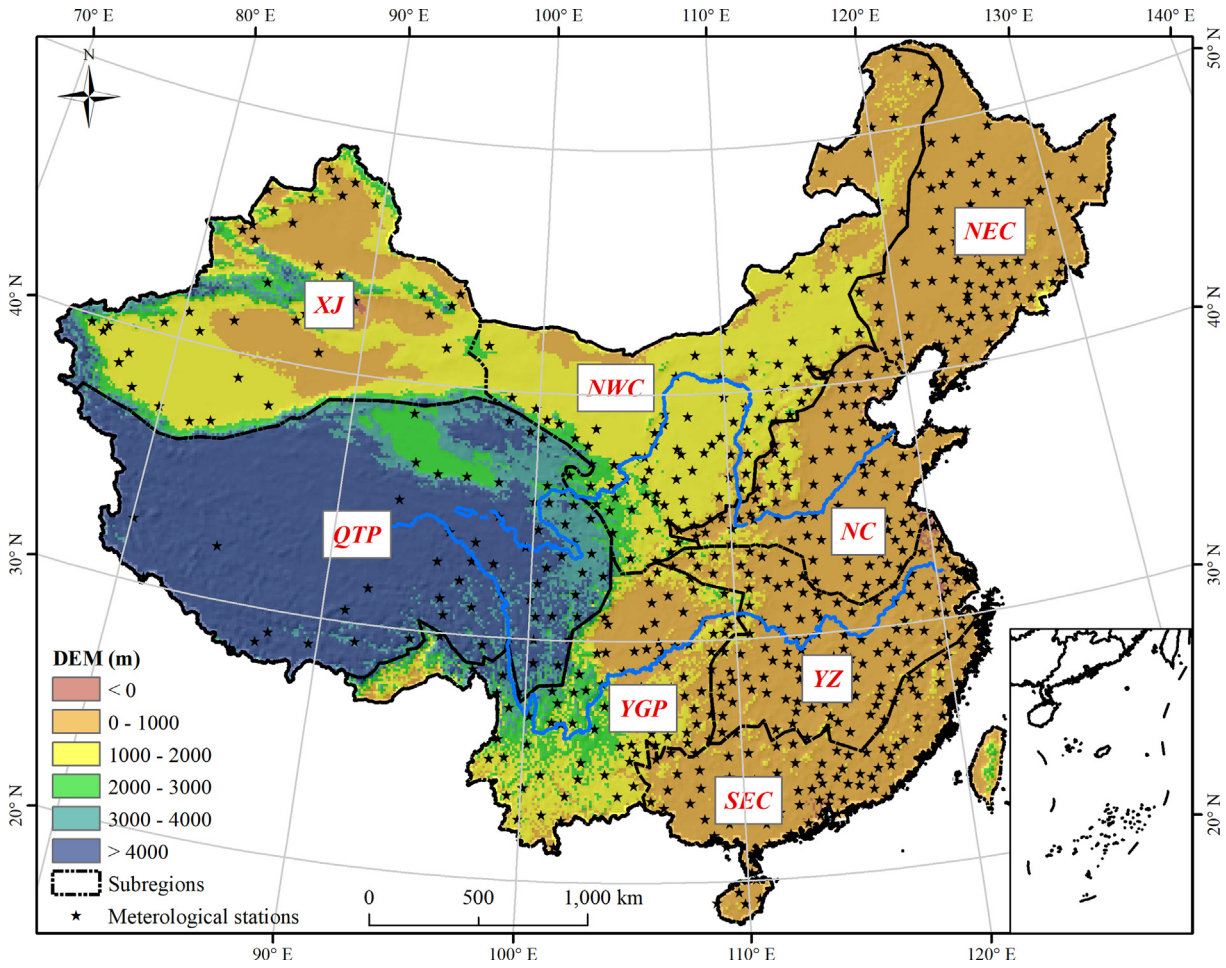

Fig. 1. Topography of China and the locations of the meteorological stations within the eight subregions across mainland China. The sub-regions are the Xinjiang region (XJ), the Qinghai-Tibetan Plateau (QTP), the middle- and downstream Yangtze River Basin (YZ), the southwest Yungui Plateau (YGP), Northwest China (NWC), Northeast China (NEC), North China (NC), and Southeast China (SEC).

covers the quasi-global areas ranging 60°N-60°S with a spatial resolution of 0.1°×0.1°, and will be extended to the fully global domain (90°N-S) in the future. IMERG has three versions (i.e., Early Run, Late Run, and Final Run) to facilitate a wide range of users. The Early Run and Late Run versions are near-real-time with a latency of 4 h and 12 h, respectively, after the satellite acquisition. The Final Run version, on the other hand, is post-real-time with a latency of 3.5 months. Different from the near-real-time product, the post-real-time one has merged monthly ground-based observations from the Global Precipitation Climatology Center (GPCC) network. The daily accumulated IMERG Early Run product (version 6, precipitationCal subset) for the period 2007–2017 was used in this study; and it was collected from the National Aeronautics and Space Administration at the Goddard Earth Sciences Data and Information Services Center (GES DISC) (https://disc.gsfc.nasa.gov/). For simplicity, it would be referred to IMERG hereafter. More information regarding the IMERG product are available in Huffman et al. (2019).

2.2.2. Bottom-up satellite precipitation product

There are currently two available bottom-up satellite precipitation products, i.e., SM2RAIN-CCI and SM2RAIN-ASCAT, which were obtained by applying the SM2RAIN algorithm (Brocca et al., 2013) to the ASCAT soil moisture observations (Wagner et al., 2012) and the European Space Agency (ESA) Climate Change Initiative combined active and passive microwave satellite soil moisture product (Dorigo et al., 2017), respectively. The SM2RAIN algorithm derives the precipitation from the soil moisture data mainly based on the soil water balance (Brocca et al., 2013). By assuming negligible runoff and evaporation during the rainy period, the precipitation (p) could be estimated using Eq. (1).

$$p(t) \cong \frac{nZds(t)}{dt} + as(t)^m \quad (1)$$

where n is the soil porosity, Z is the soil layer depth (mm), s is the relative soil moisture, t is the time (days), a and m are the parameters used to estimate drainage (deep percolation plus subsurface runoff) rate (mm/day).

The SM2RAIN-CCI product has applied a static mask to mask out the periods with high frozen soil and snow probability, rainforest areas, and the areas with high topographic complexity (Ciabatta et al., 2018), which leads to a large of missing data over mainland China. Hence, it was not used in this research. The SM2RAIN-ASCAT product is provided at the global scale with a high spatial resolution of 12.5 km and a daily temporal resolution. The newly released version of SM2RAIN-ASCAT (version 1.1), which are freely available at the website: https://zenodo.org/record/3405563, was used in this study. It should be noted that the SM2RAIN-ASCAT data has been resampled to the grids of IMERG (0.1°×0.1°) through the nearest neighboring algorithm in order to match the spatial resolutions. The SM2RAIN-ASCAT product is simply referred to SM2RASC hereafter for conciseness. More information about SM2RIN-ASCAT can be found in Brocca et al. (2019).

2.2.3. Ground-based observations

In this study, the precipitation observations from 701

meteorological stations were used to assess the performance of the SPPs. As depicted in Fig. 1, the stations are very unevenly distributed across mainland China, with a relatively high density in the subregions NEC, NC, YZ, YGP and SEC, while a relatively low density in XJ and NWC, and a lowest density on the QTP. Daily precipitation observations from the meteorological stations for the period 2007–2017, provided by the National Meteorological Information Center (NMIC) of the China Meteorological Administration (CMA), were collected from the China Meteorological Data Service Center (CMDSC) at the website: http://data.cma.cn/. The precipitations were measured mainly through the tipping bucket and weighing rain gauges (Qing et al., 2018), of which the former be used to measure liquid precipitation (i.e., rain and drizzle), while the later be used to measure solid precipitation such as snowfall, mixed rainfall and snowfall, and hail (Wang, 2017). All the precipitation measurements have undergone strict quality controls (Shen et al., 2010; Zhao and Yatagai, 2014) including (i) the extreme values' check, (ii) the spatio-temporal consistency check, (iii) the internal consistency check (e.g. duplicated data and incorrect units), and (iv) the manual inspection and correction. Hence, they are believed to be robust, and could be used as the ground reference.

The daily precipitation of the IMERG and SM2RAC products are both the accumulated data from 00:00 to 24:00 UTC. However, the observations are the accumulated precipitation between 20:00 and 20:00 (Bejing Time, UTC + 8). We, therefore, recalculated the daily precipitation observations to render them to be temporally consistent with the SPPs. This is easy to implement since that, besides the accumulated precipitation for the period 20:00–20:00 (Bejing Time, UTC + 8), the ones for the two sub-periods (i.e., 20:00 to 8:00 and 8:00 to 20:00) are also available for each day. The daily precipitation for the period 0:00–24:00 UTC could be easily obtained by adding the accumulated data between 8:00 and 20:00 (UTC + 8) in the current day, and that between 20:00 and 8:00 (UTC + 8) in the next day.

3. Methodology

3.1. Integration of the top-down and bottom-up satellite precipitation products

In this study, an additional precipitation product was generated by integrating the top-down and bottom-up satellite precipitation products (i.e., IMERG and SM2RASC). The integration was implemented through a simple nudging scheme (Massari et al., 2014; Ciabatta et al., 2015; Brocca et al., 2016), as in Eq. (2).

$$P_{\text{int}}(t) = P_{\text{IMERG}}(t) + K\left(P_{\text{SM2RASC}}(t) - P_{\text{IMERG}}(t)\right) \tag{2}$$

where $P_{\text{int}}(t)$ is the integrated precipitation, $P_{\text{IMERG}}(t)$ is the IMERG precipitation estimates, $P_{\text{SM2RASC}}(t)$ is the SM2RASC precipitation estimates, and K is the parameter that has the same role of the Kalman gain in the classic data assimilation technique (Massari et al., 2014; Huang et al., 2016). The parameter K ranges from 0 to 1; and the greater the value, the higher the weight given to SM2RASC, and lower weight given to IMERG. The rationale behind the integration algorithm is very similar with the multi-model ensemble strategy such as the simple inverse-error-square averaging and the advanced Bayesian model averaging, which assign higher weights to the better performing predictions than the worse performing ones in order to exploit the diversified capabilities of the predictions of different models (Duan et al., 2007; Shen et al., 2014; Ma et al., 2018; Mastrantonas et al., 2019). The K values were determined through a calibration process with the goal of minimizing the root mean square error (RMSE) between the observations and the integrated results. The calibration was carried out for each meteorological station during the period 2007–2011 at the daily scale by using the fmincon function in MATLAB. After calibration, the parameter K was used to estimate precipitation for the validation period 2012–2017. The integrated product would be referred to IMERG&SM2R hereafter.

3.2. Evaluation of IMERG, SM2RASC and IMERG&SM2R

The evaluations of IMERG, SM2RASC and IMERG&SM2R were conducted using the grid-to-point technique (i.e., the nearest neighbor method). More specifically, we first find out the grid of the SPPs that contains the meteorological station, and then extract the grid precipitation values, and compared them with the corresponding observations. The SPPs were quantitatively assessed through three continuous statistical measures: (i) correlation coefficient (CC); (ii) relative bias (Rbias); (iii) normalized root mean square error (NRMSE), which are defined as in Eqs.3, 4, and 5 respectively. A higher CC and a lower NRMSE together with a lower absolute Rbias signify better agreements between the precipitation estimates and the observations, and vice versa. Considering that the integrated product may inflate the performance over the calibration period, we assessed the IMERG, SM2RASC and IMERG&SM2R products for the calibration period (2007–2011) and validation period (2012–2017), respectively.

$$\text{CC} = \frac{\sum_{i=1}^{n}(P_i^{obs} - P_{mean}^{obs})(P_i - P_{mean})}{\sqrt{\sum_{i=1}^{n}(P_i^{obs} - P_{mean}^{obs})^2}\sqrt{\sum_{i=1}^{n}(P_i - P_{mean})^2}} \tag{3}$$

$$\text{Rbias} = \frac{\sum_{i=1}^{n}(P_i - P_i^{obs})}{\sum_{i=1}^{n}P_i^{obs}} \times 100\% \tag{4}$$

$$\text{NRMSE} = \frac{\sqrt{\frac{1}{n}\sum_{i=1}^{n}(P_i - P_i^{obs})^2}}{\frac{1}{n}\sum_{i=1}^{n}P_i^{obs}} \tag{5}$$

where P_i and P_i^{obs} are precipitation estimates of the SPPs and the observations, respectively, at the time step i; P_{mean} and P_{mean}^{obs} are the mean values of precipitation estimates and the observations, respectively; and n is the total number of time steps. Moreover, three categorical metrics including the probability of detection (POD), false alarm ratio (FAR) and critical success index (CSI), defined as in Eqs. (6)–(8), respectively, were employed to assess the capability of the SPPs in detecting precipitation events.

$$\text{POD} = a/(a + b) \tag{6}$$

$$\text{FAR} = c/(a + c) \tag{7}$$

$$\text{CSI} = a/(a + b + c) \tag{8}$$

where a is the number of precipitation events correctly detected; b is the number of the missed events; and c is the number of non-events that are incorrectly detected. Hence, the POD refers to the fraction of the correctly detected precipitation events; the FAR refers to the fraction of the predicted events that are erroneously detected; and the CSI is an integrated measure of the overall performance. The values of POD, FAR and CSI range from 0 to 1. Higher POD and CSI together with a lower FAR signify better performance. The categorical metrics were computed at each meteorological station for different precipitation thresholds, i.e., 1, 5, 10 and 15 mm/day.

Besides the performance metrics at the daily and monthly scales, those in different seasons, i.e., spring (March-May), summer (June-August), autumn (September-November), and winter (December-February), were also calculated in order to analyze the seasonal variations of the performance of the three SPPs. Furthermore, we depicted the performance metrics at each meteorological station over mainland China to further investigate the spatial variability of the performance. In addition, we further explored the performance dependence of the SPPs on the topography and precipitation magnitudes by conducting the correlation analyses between the performance metrics and the elevations (or the annual average precipitation).

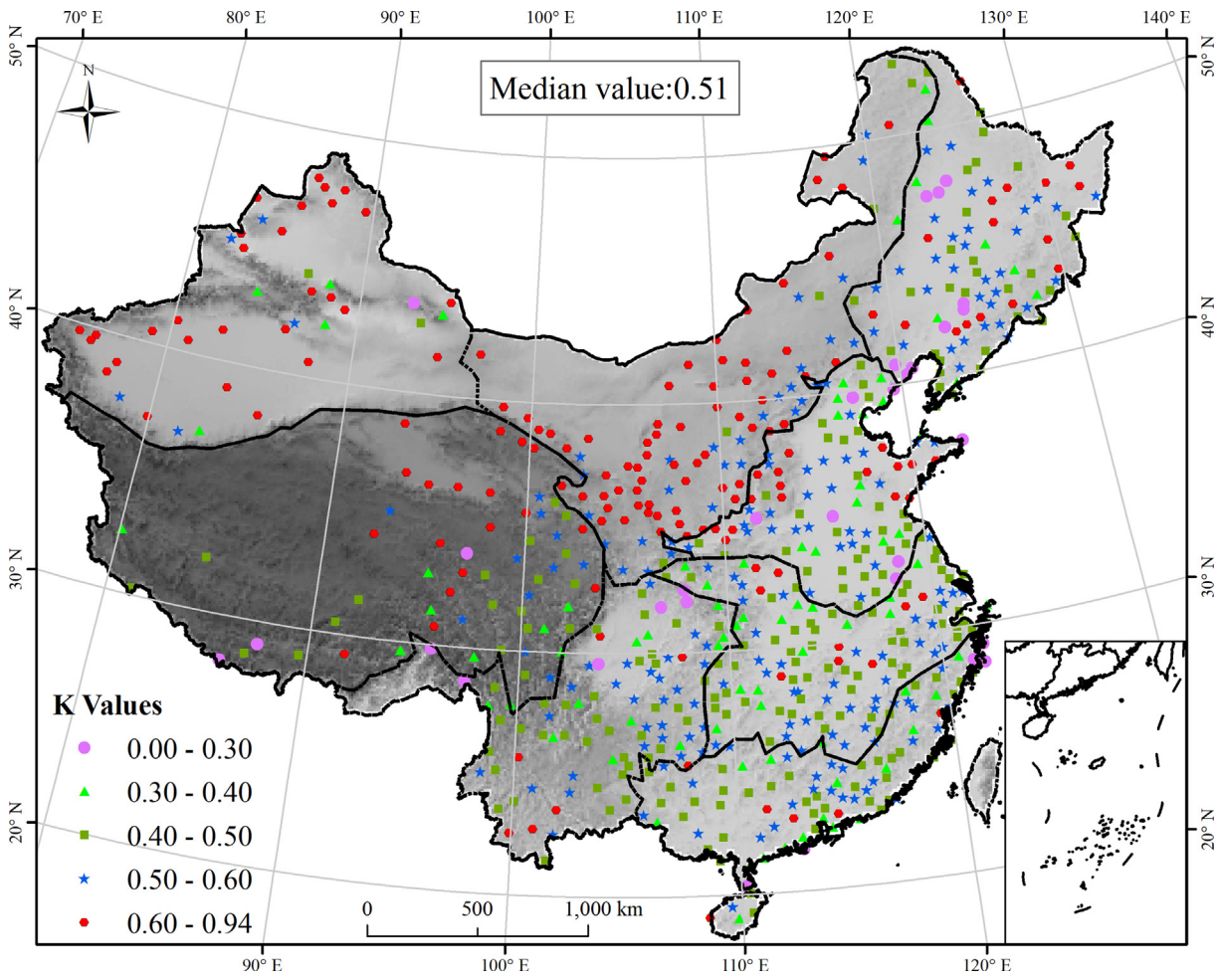

Fig. 2. Spatial variability of the parameter *K* of the integration algorithm.

4. Results

4.1. Calibration of the integration algorithm

The spatial variability of the calibrated parameter *K* of the integration algorithm (Eq.2) is shown in Fig. 2. It is seen that the parameter *K* is greater than 0.5 at most of the stations within the subregions XJ and NWC, indicating that, overall, higher weights have been given to the SM2RASC product in the process of integration. However, they mainly range 0.3 to 0.6 within the subregions YZ, SEC and YGP, implying that, overall, higher weights have been given to IMERG. In the remaining subregions (i.e., QTP, NEC and NC), the parameter *K* varies greatly, and shows obviously stronger spatial variability than the other subregions. The median value of the parameter *K* is 0.51, suggesting that the integrated product originates almost equally from SM2RASC and IMERG over mainland China.

4.2. Performance assessment over mainland China

4.2.1. Continuous performance metrics

Fig. 3 presents the box plots of the continuous performance metrics for IMERG, SM2RASC and IMERG&SM2R at the daily scale during the calibration and validation periods, respectively. The median CC is 0.65 (or 0.67) for IMERG, while it is 0.56 (or 0.58) for SM2RASC during the calibration (or validation) period. Hence, SM2RASC performs worse than IMERG at the daily scale, in terms of CC. However, the median NRMSE is almost the same for IMERG and SM2RASC in both the calibration and validation periods. This suggests that there is a larger systematic error and a lower random error in IMERG, in comparison to SM2RASC. The results at the monthly scales are plotted in Fig. 4. The median CC are 0.83 and 0.87, respectively, for IMERG and SM2RASC during the calibration period, and they are 0.83 and 0.85, respectively, during validation period. The median NRMSE values are 0.67 (or 0.65) and 0.59 (or 0.58), respectively, for IMERG and SM2RASC, during the calibration (or validation) period. Hence, unlike the results at the daily scale, SM2RASC performs better than IMERG at the monthly scale. In terms of Rbias, the median values are 8.65% and 11.18%, respectively, for IMERG during the two sub-periods, indicating an overestimation of precipitation. However, the Rbias is tiny (0.36%) for SM2RASC during the calibration period, while it is −3.40% during the validation period. Regarding the integrated product IMERG&SM2R, it could increase the median CC by 9.23% (or 8.43%) and 26.79% (or 3.45%), respectively, compared to IMERG and SM2RASC, respectively, for the daily (or monthly) precipitation in the calibration period. Meanwhile, it could reduce the NRMSE by 16.90% (or 16.61%) and 26.87% (or 16.95%), respectively. Very similar results can be observed for the validation period. These results indicate that IMERG&SM2R has an obviously improved performance, in comparison to its parent products (i.e., IMERG and SM2RASC).

4.2.2. Categorical performance metrics

Fig. 5 shows the box plots of the categorical metrics POD, FAR and CSI for the SPPs with the precipitation thresholds of 1, 5, 10 and 15 mm/day, respectively. In the calibration period, the median POD is 0.73 for IMERG with the precipitation threshold of 1 mm/day, lower than that for SM2RASC (0.82). However, the median FAR is 0.56 for

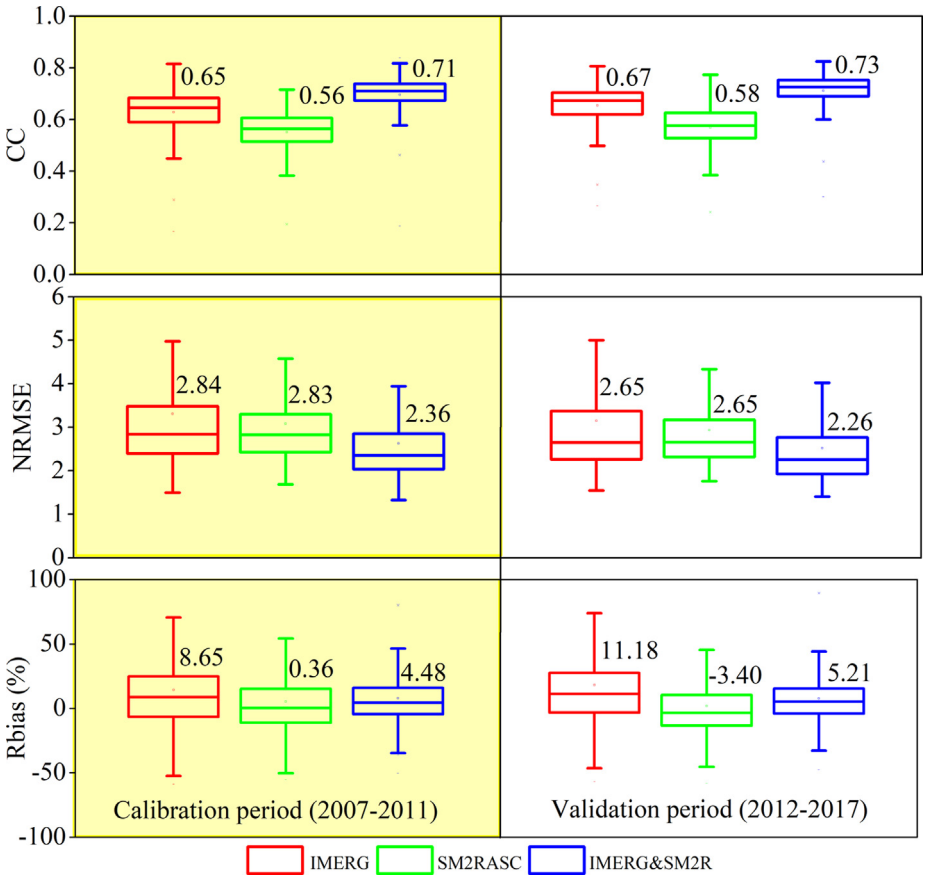

Fig. 3. Box plots of the continuous performance metrics for IMERG, SM2RASC and IMERG&SM2R at the daily scale in the calibration and validation periods. The median values of the performance metrics are presented at the top of each box.

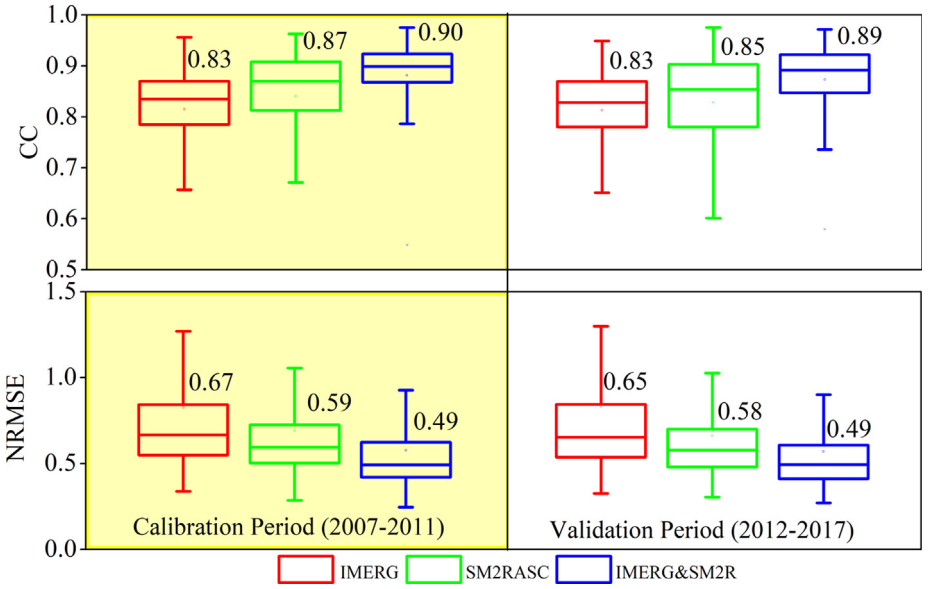

Fig. 4. Box plots of the continuous performance metrics for IMERG, SM2RASC and IMERG&SM2R at the monthly scale in the calibration and validation periods.

SM2RASC, obviously higher than that for IMERG (0.41). This leads to a higher value of the CSI for IMERG than SM2RASC, which are 0.47 and 0.39, respectively, in line with the results when the precipitation threshold increases to 5 mm/day. The median POD, FAR and CSI are 0.56 (or 0.51) , 0.45 (or 0.49) and 0.48 (or 0.34), respectively, for IMERG, and are 0.43 (or 0.27), 0.49 (or 0.47) and 0.30 (or 0.21), respectively, for SM2RASC when the threshold is set as 10 mm/day (or 15 mm/day) in the calibration period. Hence, SM2RASC performs better (or worse) than IMERG in terms of POD (or FAR) when the precipitation threshold is < 10 mm/day, while vice versa is the case when the threshold is 10 or 15 mm/day. The very similar results can be found for the validation period. Nevertheless, IMERG outperforms SM2RASC for all the precipitation thresholds in terms of CSI. Regarding the integrated product IMERG&SM2R, the median POD is consistently

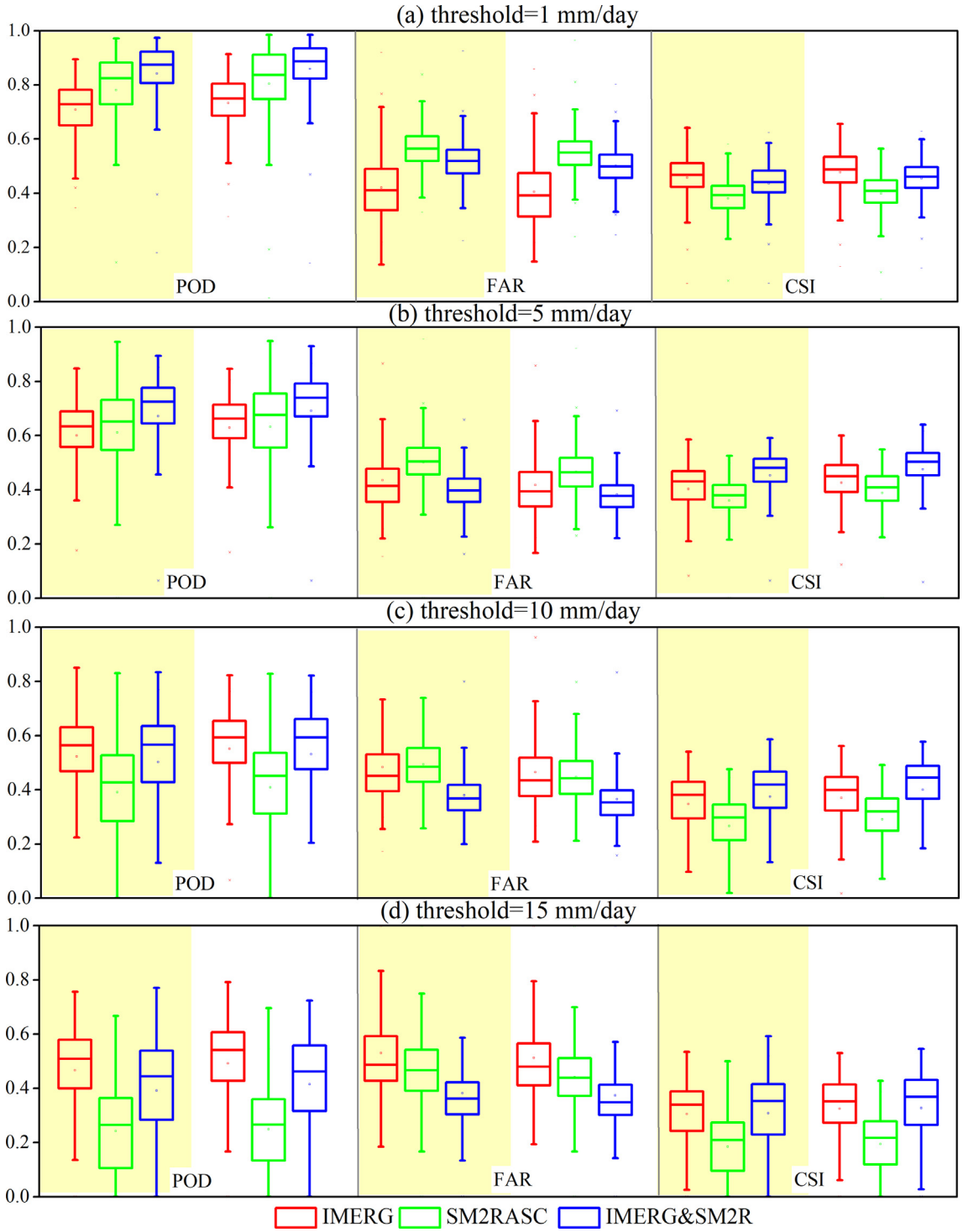

Fig. 5. Box plots of the categorical metrics for IMERG, SM2RASC and IMERG&SM2R with different precipitation thresholds. The yellow and white panels show the results in the calibration and validation periods, respectively. (For interpretation of the references to colour in this figure legend, the reader is referred to the web version of this article.)

higher than its parent SPPs when the threshold is < 10 mm/day, while the median FAR is consistently lower than its parent products when the threshold is higher than 5 mm/day. Overall, the IMERG&SM2R product outperforms its parent SPPs in detecting precipitation events when threshold is higher than 1 mm/day, as indicated by the higher CSI values. The median CSI could be increased by IMERG&SM2R with the magnitudes of 3.78–11.69% and 26.75–68.66%, respectively, compared to SM2RASC and IMERG, respectively, in the calibration period. As shown in Fig. 5, the categorical metrics for IMERG, SM2RASC and IMERG&SM2R in the validation period are very closed to the calibration period.

4.3. Seasonal variability of the performance

As shown in Fig. 6, the IMERG, SM2RASC and IMERG&SM2R products show similar seasonal variability regarding the performance at the daily scale. In terms of CC, it has higher values in summer and autumn than in winter. The median NRMSE, on the contrary, is the

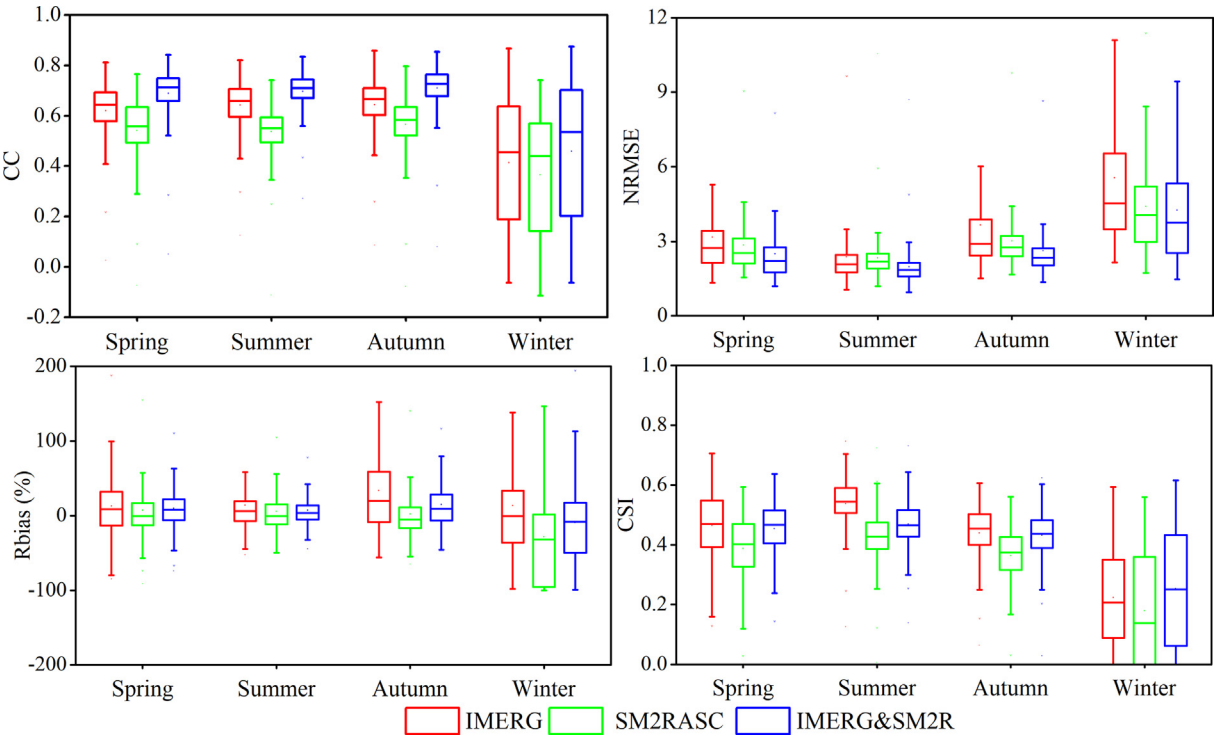

Fig. 6. Seasonal variations of the performance metrics for IMERG, SM2RASC and IMERG&SM2R at the daily scale.

largest in winter, and is the lowest in summer. The median CC for IMERG is higher than SM2RASC in all seasons. The median NRMSE for SM2RASC is consistently lower than IMERG in spring, autumn and winter, while the contrary is the case in summer. The Rbias shows relatively small seasonal variations. Nevertheless, it has obviously larger ranges in winter, with a lower median value compared to the other seasons. In terms of CSI, it has the highest median value in summer, followed by autumn, spring and winter. The IMERG product has a better ability in detecting precipitation events than SM2RASC in all seasons, as indicated by the higher CSI values. The seasonal variations of the performance metrics for the three SPPs at the monthly scale, not shown here, are in consistent to those at the daily scale, with the difference that SM2RASC performs better than IMERG in all season while the contrary is the case at the daily scale. The integrated product IMERG&SM2R performs the best among the three SPPs in all seasons at both the daily and monthly scales, as indicated by the higher CC and CSI values and lower NRMSE relative to the parent SPPs (i.e., IMERG and SM2RASC).

4.4. Spatial variability of the performance over mainland China

Fig. 7 plots the spatial patterns of the performance metrics for IMERG, SM2RASC and IMERG&SM2R at the daily scale. In terms of CC, it shows relatively high values for IMERG in the humid subregions SEC, YGP and YZ, followed by NC, NEC and NWC. The arid subregions XJ have the lowest CC on average, compared to the other subregions. Overall, the CC decreases from the humid southeast China to the arid and semi-arid regions of northwest China for the IMERG product. Regarding the SM2RASC product, however, the CC have higher values in the semi-arid subregion NWC, in comparison to the other subregions. The lowest CC can be similarly observed in the arid subregion XJ. In terms of NRMSE, it decreases obviously from northwest to southeast China for both IMERG and SM2RASC. The subregions XJ and NWC have higher NRMSE values while the subregions SCE, YZ and YGP have relatively lower NRMSE values. The Rbias is positive for the IMERG product within most of the subregions of mainland China except for QTP, over which the Rbias is negative, and with higher magnitudes (< -20%). With respect to SM2RASC, the Rbias is negative at most of the stations within the subregions NEC, YZ and NC. The Rbias has large variability for SM2RASC over the remaining subregions, within which both positive and negative values are widely distributed. The CSI values were calculated for the three SPPs with the precipitation threshold of 1 mm/day. They are relatively high (greater than0.50) in YZ and SEY, but low (< 0.30) in XJ for the IMERG product. For the SM2RASC product, the CSI shows high values in YZ, SEC and QTP, and similarly, has the lowest values in XJ. As depicted in Fig. 7, the spatial patterns of CC, Rbias and CSI for the integrated product IMERG&SM2R agree well with IMERG. The NRMSE for IMERG&SM2R is obviously lower than those for IMERG and SM2RASC in the subregions YZ and SEC, indicating a substantial improvement of the performance. Comparing the results for the three SPPs, we can conclude that the integrated product performs better than IMERG and SM2RASC at most of the stations over mainland China, as indicated by the higher CC and lower NRMSE values, together with the lower absolute Rbias values. Meanwhile, IMERG overall outperforms SM2RASC in the humid subregions (i.e., NEC, YZ and YGP), while it performs worse than SM2RASC in the semi-arid region (i.e., NWC).

Fig. 8 depicts the spatial distributions of the CC and NRMSE for the three SPPs at the monthly scale. The CC shows high values (greater than0.70) for the IMERG and SM2RASC products across mainland China except for the subregion XJ. The higher CC at the monthly scale than the daily one can be explained by the fact both IMERG and SM2RASC have been subjected to a static monthly climatological correction (Brocca et al., 2019; Huffman et al., 2019); and meanwhile, the variability of the monthly precipitation is considerably lower than the daily one. In terms of NRMSE, in line with the results at the daily scale, it decreases form southeast to northwest China for both IMERG and SM2RASC. The CC and NRMSE maps of IMERG&SM2R are different from those of IMERG and SM2RASC, with obviously more stations have higher CC and lower NRMSE values. Overall, the performance metrics for the three SPPs have strong spatial variability at both daily and monthly scales. However, the spatial patterns diverge significantly between the three SPPs. On average, IMERG and IMERG&SM2R perform better in the humid subregions (i.e., YZ, SEC and YGP) than in the arid

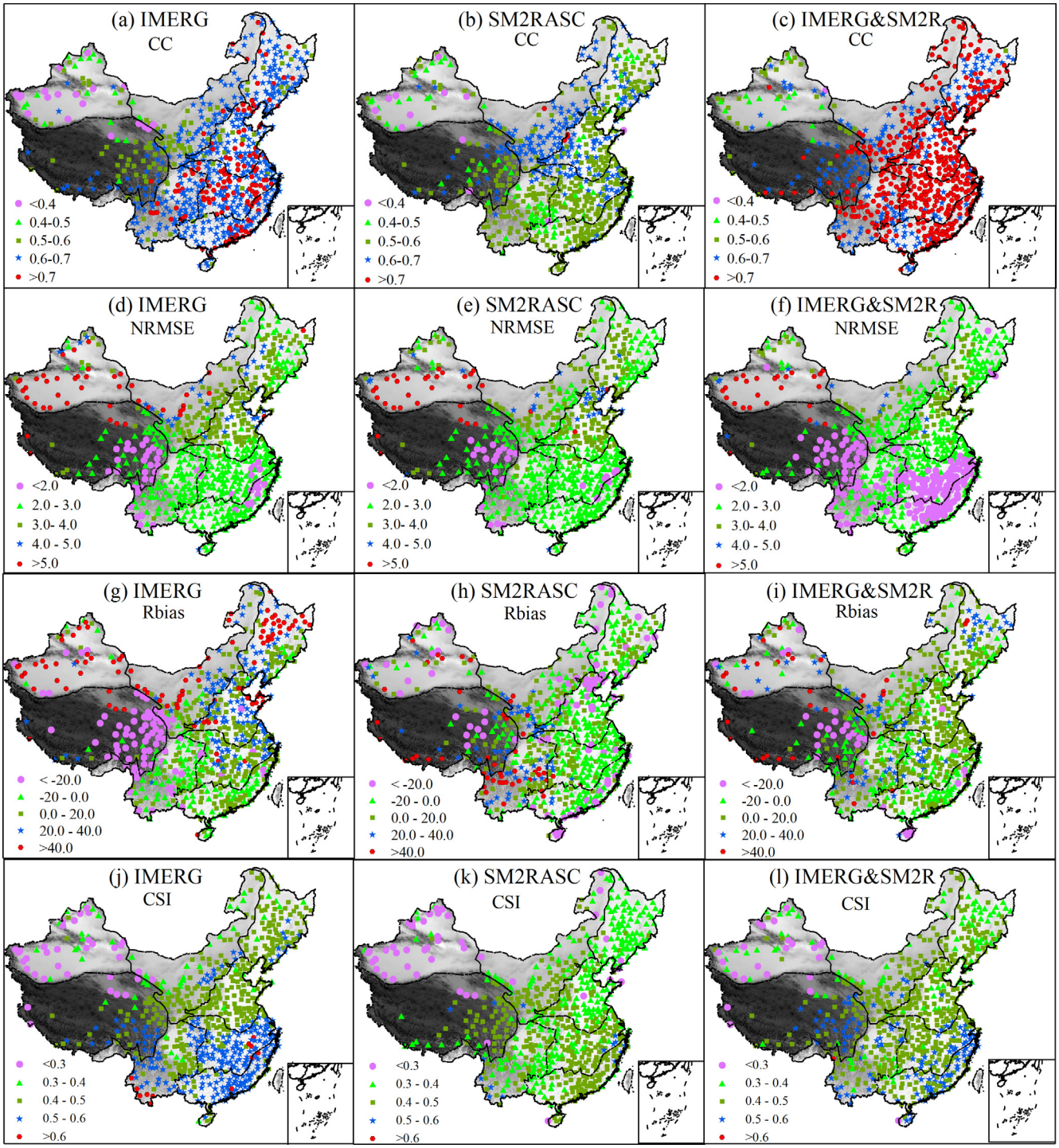

Fig. 7. Spatial patterns of the performance metrics for IMERG, SM2RASC and IMERG&SM2R at the daily scale. The four rows display the CC, NRMSE, Rbias and CSI, respectively.

and semi-arid subregions (i.e., NWC and XJ) and the QTP. However, SM2RASC perform better in semi-arid subregion NWC than the remaining subregions.

4.5. Performance dependence on the elevations and precipitation magnitudes

Fig. 9 shows the correlations of the performance metrics with the elevations for IMERG, SM2RASC and IMERG&SM2R, respectively, at the daily scale. The CC consistently shows a significant negative correlation with the elevations for the three SPPs. In terms of NRMSE, however, it presents an insignificant correlation with the elevations for all the three SSPs. The Rbias and CSI decrease significantly with the increasing elevations for IMERG. However, the Rbias increases significantly, and the CSI decrease insignificantly for SM2RASC. The correlations of Rbias and CSI with the elevations are not significant for the integrated product. The results at the monthly scale are shown in Table 1. Different from those at the daily scale, the CC shows a positive correlation with the elevations for the three SPPs, and meanwhile, the NRMSE correlates significantly with the elevations for the SPPs. Fig. 10

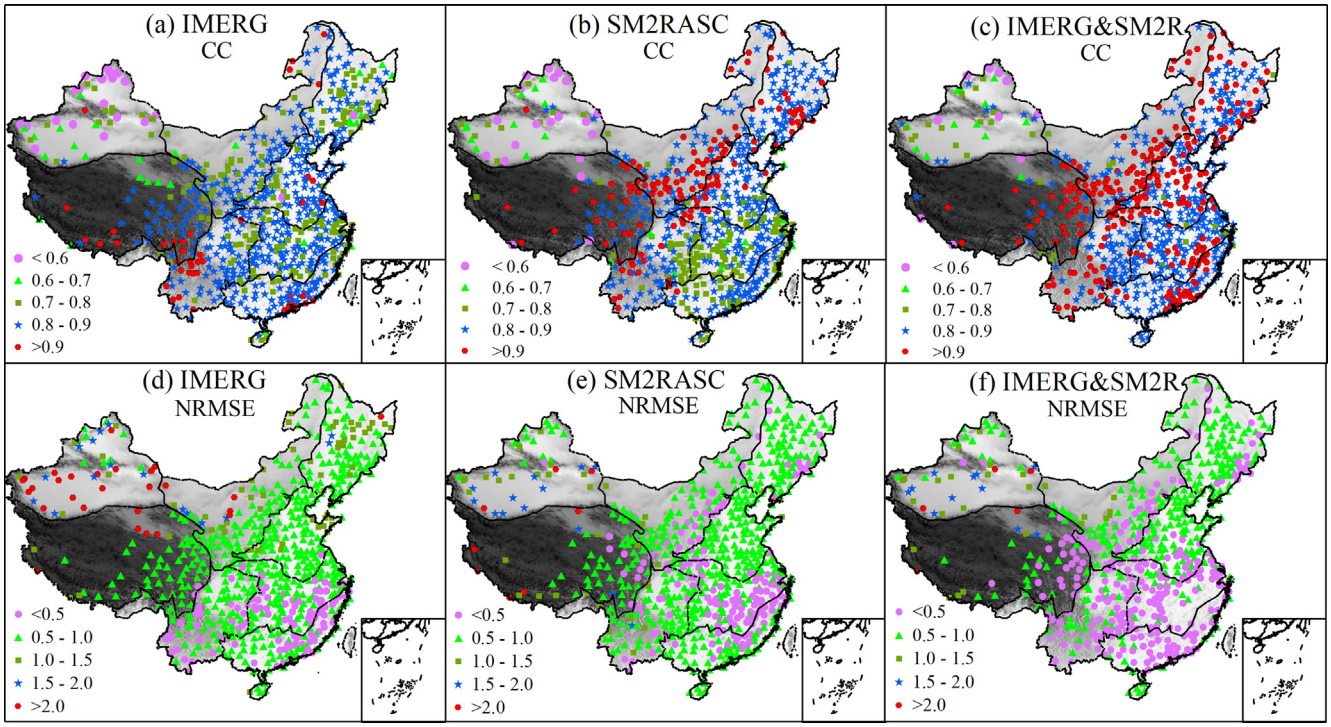

Fig. 8. Spatial patterns of the performance metrics (CC and NRMSE) for IMERG, SM2RASC and IMERG&SM2R at the monthly scale.

plots the relationships between the performance metrics and the annual precipitation magnitudes at the daily scale. The CC shows a significant positive correlation with the elevations for IMERG and IMERG&SM2R, while it has an insignificant one for SM2RASC. The NRMSE and Rbias present significant downward trends, while the CSI exhibits a significant upward trend with increasing precipitation magnitudes for all the three SPPs. The absolute Rbias tends to decrease with increasing precipitation magnitudes for IMERG and IMERG&SM2R, while it tends to increase for SM2RASC. At the monthly scale, the CC correlates positively with the precipitation magnitudes for IMERG and IMERG& SM2R, whereas it shows an insignificant correlation for SM2RASC. In terms of NRMSE, it consistently correlates negatively with precipitation magnitudes for the three SPPs at the daily and monthly scales. Overall, these results demonstrate that the performance of the three SPPs depends greatly on the elevations and precipitation magnitudes.

5. Discussion

5.1. Comparisons of the performances of IMERG and SM2RASC

In this study, we assessed the bottom-up SM2RASC product and the top-down IMERG product over mainland China in a timely manner. The IMERG product has a better performance than SM2RASC in terms of CC at the daily scale, which is different from a similar study conducted over the southern Italy (Chiaravalloti et al., 2018) which reported an almost comparable performance of the two SPPs. In contrast, IMERG performs worse than SM2RASC at the monthly scale. The inconsistent performance at the daily and monthly scales is possibly due to the better capabilities of SM2RASC in retrieving accumulated rainfall, and meanwhile, the stable product accuracy of SM2RASC over time (Brocca et al., 2019). Meanwhile, the monthly climatological corrections based on different benchmarks might also contribute to explain the inconsistency. The IMERG product was calibrated against the Global Precipitation Climatology Project (GPCP) data (Huffman et al., 2019), while SMRASC was corrected based on the ERA5 reanalysis data (Brocca et al., 2019). It should be mentioned that the climatological correction is static (or constant) for each month, which is different from the dynamic month-by-month correction implemented for the post-real-time IMERG product. In terms of the capacity in detecting precipitation events, the results indicate that IMERG achieved a better performance than SM2RASC, which disagrees with the study of Chiaravalloti et al. (2018). We also found that the POD and CSI values drop with the increasing precipitation thresholds for both SPPs, indicating a deteriorate performance for detecting more intense precipitation events, as reported in some other studies (e.g. Li et al., 2018; Rozante et al., 2018).

Both IMERG and SM2RASC show obvious seasonal variability of the performance. They tend to have better performance in the wet seasons (summer and autumn) than the dry seasons (winter and spring), as reported in the previous studies (e.g. Wei et al., 2018; Paredes-Trejo et al., 2019; Wang et al., 2019a). In winter, SM2RASC tend to underestimate precipitation significantly, as indicated by the high negative median Rbias (–32.15%). The underestimation by SM2RASC is possibly due to the deficiency of the SM2RAIN algorithm (Brocca et al., 2013) which retrieve precipitation mainly depends on the soil moisture variations. In winter, the rainfall on the frozen soil might not be able to induce detectable soil moisture variation for the sensor (i.e., ASCAT) on board the satellite, resulting in the misses of some precipitation events. Moreover, the SM2RAIN algorithm could not estimate snowfall (Brocca et al., 2019), which can also explain the underestimations of precipitation in winter.

The IMERG and SM2RASC products also exhibit strong spatial variability of the performance. The IMERG product tends to have an obviously better performance in southeast China (i.e., SEC, YZ and YGP), characterized by a humid climate, than in northwest China (i.e., XJ and NWC) that is controlled by arid and semi-arid climates. In contrast, the SM2RASC product performs better in the semi-arid region (i.e., NWC) than in the humid subregions. This might be explained by the fact that the SM2RAIN algorithm can hardly estimate precipitation when the soil is close to saturation since the soil moisture would be constant in this case (Brocca et al., 2014). Compared to the semi-arid region, the soil over humid subregions (i.e., SEC, YGP and YZ) are more likely to experience saturation due to the more frequent precipitation events with higher magnitudes and durations. The lower performance for the SM2RAIN-derived products in the wetter regions has also been

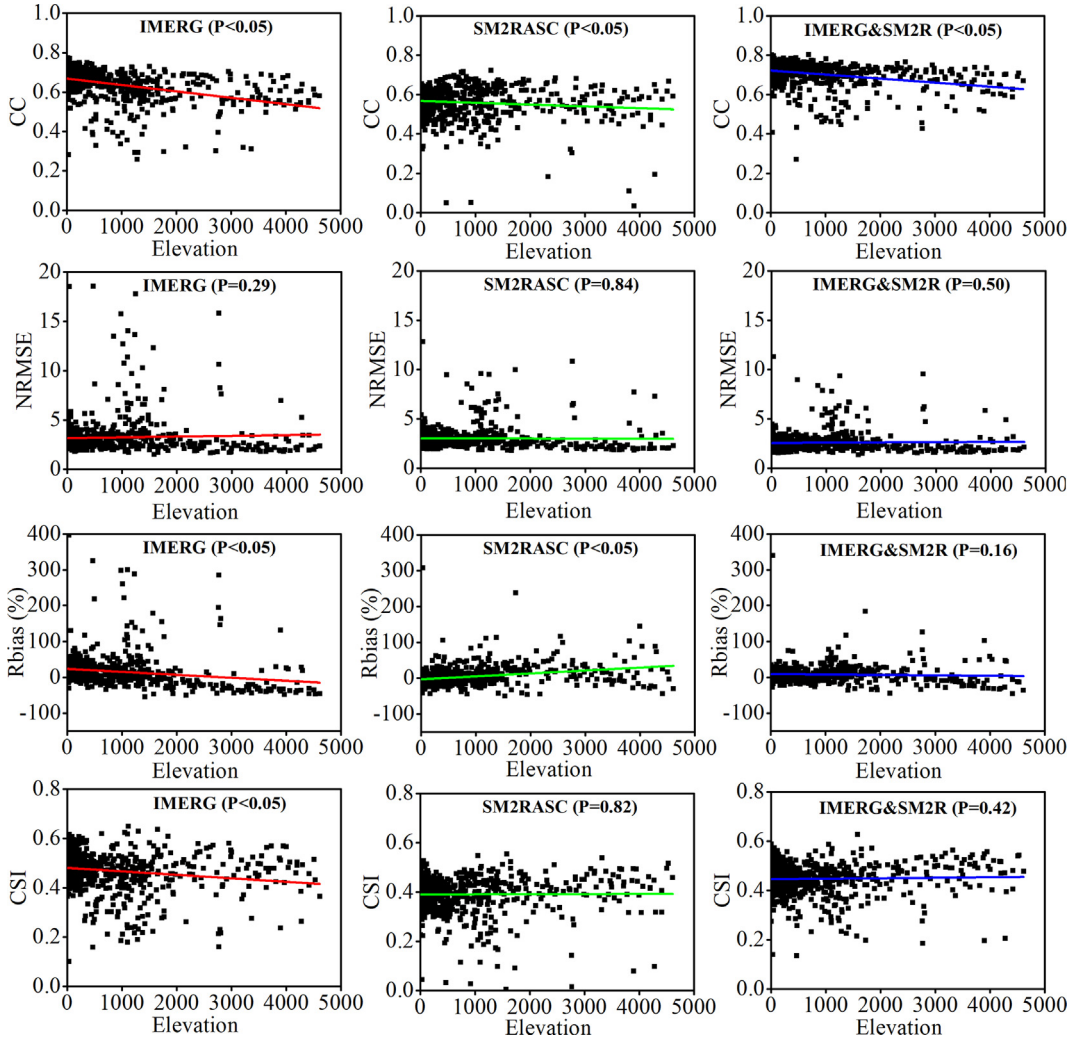

Fig. 9. Correlations of the performance metrics with the elevations for IMERG, SM2RASC and IMERG&SM2R at the daily scale. The significance of the correlations (i.e., the P values) are also presented in the figure.

reported in the previous studies (Paredes-Trejo et al., 2019; Rahman et al., 2019a). The SM2RASC product performs worse in the arid region (i.e. XJ) relative to the other subregions, in line with Paredes-Trejo et al. (2018). This might be due to the deficiency of the ASCAT product in estimating soil moisture under the dry climatic conditions. The strong spatial variability of the performance of IMERG and SM2RASC indicates that whether the former outperforms the later or not depends heavily on the regions to be studied, which highlights the necessity of conducting a preliminary evaluation of the SSPs before their applications.

The further analyses revealed that the performances of IMERG and SM2RASC are closely correlated to the elevations and precipitation magnitudes, agreeing with the studies of Bharti and Singh (2015) and Xu et al. (2017). The correlations, however, can vary significantly between IMERG and SM2RASC, different time scales and different evaluation metrics. The performances for IMERG and SM2RASC tend to decrease from the high-altitude regions to the low-altitude regions in terms of CC and CSI at the daily scale. This is reasonable considering that both IMERG and SM2RASC have not taken the topographical factors into account, and meanwhile, could not deal well with the frozen and snow surfaces. With the increasing precipitation magnitudes, the IMERG product exhibits significantly better performances in terms of CC, NRMSE and CSI. The SM2RASC product, however, shows an insignificant dependence on the precipitation magnitudes in terms of CC. Meanwhile, it has a significant deteriorate performance in terms of Rbias, but a significant improved performance in terms of NRMSE and CSI with the increasing precipitation magnitudes.

Table 1
Correlations of the performance metrics with the elevations and precipitation magnitudes for IMERG, SM2RASC and IMERG&SM2R at the monthly scale.

Products	Performance metrics vs Elevation/precipitation			
	CC vs Elevation	CC vs Precipitation	NRMSE vs Elevation	NRMSE vs Precipitation
IMERG	+ (P = 0.32)	+(P < 0.05)	+ (P < 0.05)	- (P < 0.05)
SM2RASC	+ (P < 0.05)	- (P = 0.28)	+ (P < 0.05)	- (P < 0.05)
IMERG&SM2R	+ (P < 0.05)	+(P < 0.05)	+ (P < 0.05)	- (P < 0.05)

Note: the signs '+' and '-' means positive and negative correlations, respectively; P is the significance of the correlations.

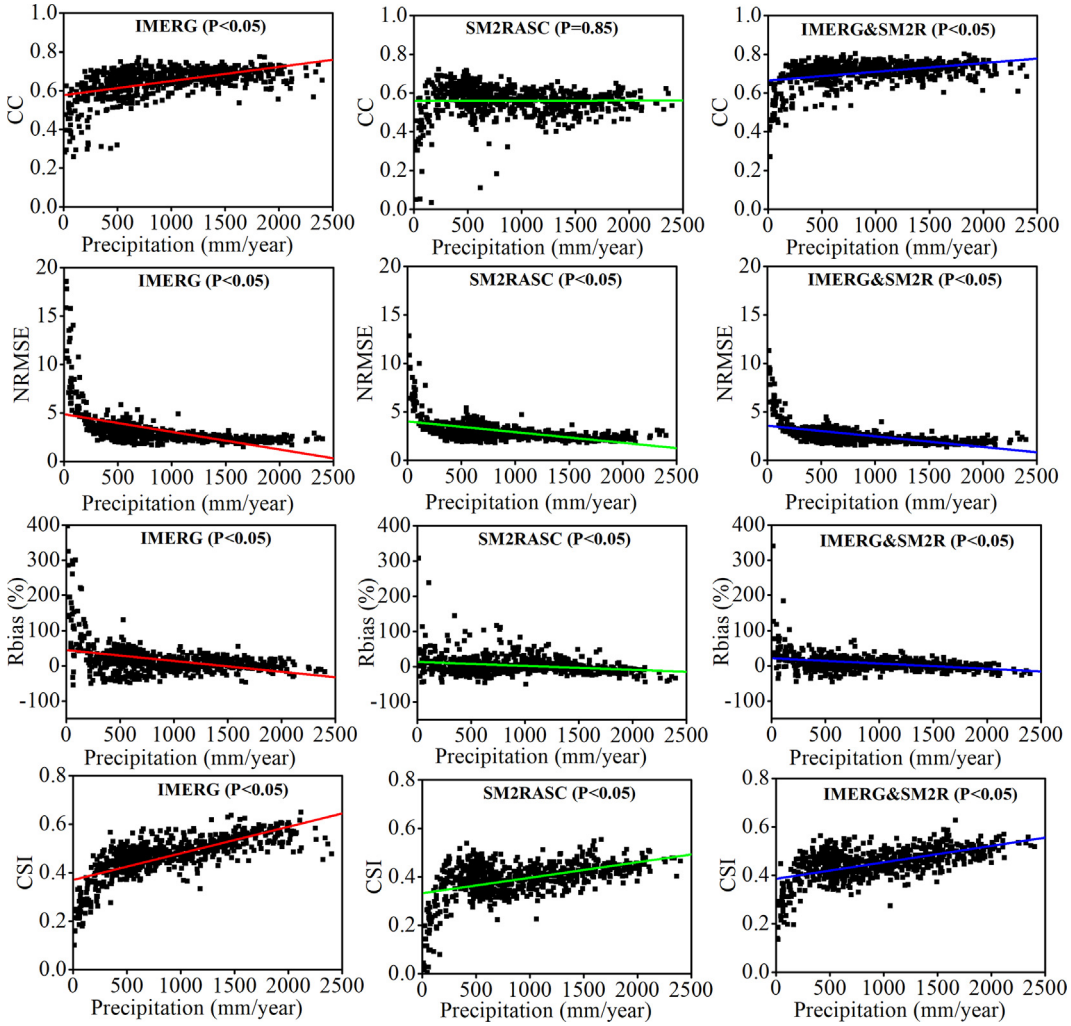

Fig. 10. Correlations of the performance metrics (CC, NRMSE, Rbias and CSI) with the precipitation magnitudes for IMERG, SM2RASC and IMERG&SM2R at the daily scale. The significance of the correlations is also presented in the figure.

5.2. Performance improvements for the integrated product

We merged the IMERG and SM2RASC products through a nudging scheme. In the calibration (or validation) period, the integrated product (i.e., IMERG&SM2R) could increase the median CC by up to 26.79% (or 25.86%) and 8.43% (or 7.23%), respectively, at the daily and monthly scales, compared to the parent products. Meanwhile, the median NRMSE could be reduced by up to 16.95% (or 14.72%) and 26.87% (or 24.62%), respectively, at the daily and monthly scales. Additionally, the median CSI could be increased by up to 68.66% (or 70.07%) when the precipitation threshold is greater than 1 mm/day in the calibration (or validation) period. These results imply the strong benefits of integrating the bottom-up and top-down SPPs, and confirmed the findings of the previous studies (e.g. Ciabatta et al., 2015; Brocca et al., 2016; Ciabatta et al., 2017; Chiaravalloti et al., 2018). This is reasonable considering that the deficiencies of one SPP could be compensated by the other one (Ciabatta et al., 2017). For instance, the deficiency of the bottom-up product SM2RASC in capturing precipitation under wet conditions can be overcame by IMERG, as proved in this study.

The integration of IMERG and SM2RASC was implemented for the daily precipitation. The integrated product also shows an improved performance at the monthly scale, compared to the parent products. This is reasonable considering that the spatial patterns of the performance of IMERG and SM2RASC at the daily scale agree well with those at the monthly scale. However, it should be mentioned that the condition may change if the post-real-time IMERG product is used. Since the post-real-time product has merged monthly ground-based observations, the spatial patterns of its performance might diverge obviously between the daily and monthly scales, depending on the number of gauge stations included in the GPCC network. In this case, the integration at the daily scale may not necessarily bring an improvement of the performance at the monthly scale.

The parameter of the integration algorithm shows strong spatial variability, and therefore, needs to be calibrated with the ground-based observations. Hence, the adopted integration algorithm can hardly be used to merge the SPPs over the ungauged regions. One possible way to address this problem is to interpolate the parameters over the spatial domain, which, however, might bring about additional biases, particularly in the mountainous areas with complex terrains. Moreover, the median value of the integration parameter K is about 0.5 in this study. This indicates the merging of IMERG and SM2RASC can be implemented through the simple arithmetic average of the two products over mainland China, as did by Chiaravalloti et al. (2018). This simple approach, therefore, could be another way to implement the integration of the SPPs over the ungauged regions. This efficacy of this approach, however, depends greatly on the regions to be studied, as well as the SPPs to be integrated.

5.3. Uncertainties

The spatial mismatch between the satellite precipitation estimates and the ground-based observation is one of the intractable issues for the evaluations of the SPPs. In this study, we adopted a grid-to-point approach, i.e., the nearest neighbor method, to evaluate the performance of IMERG and SM2RASC at each meteorological station with the assumption that the point-scale precipitation measurements are equal to the grid averages, as did in many other studies (e.g. Li et al., 2013; Ebrahimi et al., 2017; Hu et al., 2018; Yuan et al., 2018; Jiang and Bauer-Gottwein, 2019). The assumption behind the nearest neighbor method is reasonable in the flat areas with relative uniform precipitation patterns, whereas it might not hold true in the mountainous areas with complex topography and nonhomogeneous precipitation patterns. For instance, if one gauge locates in the valley of a mountainous grid of the SPPs, which is in accordance with the realities in most cases due to challenges of establishing and maintaining a gauge over the alpine areas, it may not be able to capture precipitation for the entire grid. Hence, the nearest neighbor method might induce some uncertainties to the results, particularly in the high-altitude regions such as the QTP. Moreover, the ground-based precipitation observations were implicitly assumed to be robust and error-free. However, they are likely to be subjected to various biases such as the wetting and evaporation losses, wind-induced undercatch, and underestimation of trace precipitation (Ye et al., 2004), which might be another important source of the uncertainties. In addition to the grid-to-point methods, the another avenue to evaluate the SPPs is first to interpolate the precipitation observations to the grids of the SPPs, and then compare them with the precipitation estimates of the SPPs at each grid, as did in many previous studies (e.g. Chen and Li, 2016; Tang et al., 2016; Chiaravalloti et al., 2018; Paredes-Trejo et al., 2019). This approach has not been adopted in this study considering that the interpolation algorithms could bring some additional errors and uncertainties to the performance assessments (Hu et al., 2018), especially in the regions with complex terrains and sparse rain gauges such as the QTP and XJ.

As mentioned before, the national-level meteorological stations are very unevenly distributed over mainland China. The density is relatively high in southeast China, while it is low in northwest China and the QTP. The varying densities of the precipitation gauges might also be an important source of the uncertainties. The terrains over southeast China are relatively flat, which, together with the high-density gauge networks, could result in a robust evaluation of the SPPs. However, the terrains over the northwest China and the QTP are relatively complex, which is accompanied with low-density gauge networks, and could bring large biases to the performance evaluations. Tian et al. (2018) have investigated the dependency of the performance assessments on the gauge density, and found a low-density gauge network tends to underestimate the performance of IMERG, which has also been reported by Tang et al. (2018). This highlighted that a higher-density precipitation network is more desirable for an accurate and robust assessment of the SPPs. Hence, we highly recommended to carry out more regional evaluations of the SPPs by using the observations from not only the easily accessible national-level rain gauges, but also some local-level ones, which together would generate a denser gauge network.

6. Conclusions

In this study, we evaluated and integrated two state-of-the-art SPPs, i.e., SM2RAIN-ASCAT (SM2RASC) and IMERG, over mainland China by using the ground-based observations from 701 meteorological stations. The primary difference between the two SPPs lies in that SM2RASC is obtained from the satellite soil moisture data through an innovative and bottom-up approach, while IMERG is obtained through the conventional and top-down manner. The two SPPs were integrated through a nudging scheme, resulting in an additional merged product IMERG&SM2R. The performance of IMERG and SM2RASC as well as the merged product were evaluated and compared by using both the continuous measures (i.e., CC, NRMSE and Rbias) and categorical metrices (i.e., POD, FAR and CSI). The evaluations were carried out for the calibration period (2007–2011) and validation period (2012–2017) of the integration algorithm, respectively. Further, the seasonal and spatial variabilities of the performance, and the performance dependence on the elevations and precipitation magnitudes were further explored.

Results indicate that, in terms of CC, IMERG outperforms SM2RASC, while, interestingly, vice versa is the case at the monthly scale. In terms of NRMSE, SM2RASC shows a comparable performance with IMERG at the daily scale, while it exhibits a better performance than IMERG at the monthly scale. Regarding the capability in detecting precipitation events, IMERG also achieves a better performance than SM2RASC, as indicated by the higher CSI values. Spatially, the IMERG product overall outperforms SM2RASC in the humid subregions (i.e., SEC, YZ and YGP), but it performs worse than SM2RASC in the semi-arid subregion (i.e., NWC). Both IMERG and SM2RASC show pronounced seasonal and spatial variabilities regarding the performance. They tend to perform better in the wet seasons (summer and autumn) than in the dry seasons (winter and spring). In terms of CC, the IMERG product performs better in the humid subregions than in the semi-arid subregions, followed by the complex mountainous subregion QTP and the arid subregion XJ, while SM2RASC performs better in the semi-arid subregion than the other subregions. Both of them perform relatively worse in XJ and QTP. The further analyses demonstrate that the performance of the SPPs are closely correlated to the elevations and precipitation magnitudes. The correlations and their significances, however, vary between IMERG and SM2RASC, and between different time scales and different evaluation metrics.

The integrated product IMERG&SM2R outperforms its parent products significantly. In the validation period 2012–2017, it could increase the median CC by up to 25.86% and 7.23%, respectively, at the daily and monthly scales, and reduce the median NRMSE by up to 14.72% and 24.62%, respectively, compared to the parent products. Moreover, the median CSI could be increased by 4.80–70.07% when the precipitation threshold is greater than 1 mm/day. The results demonstrate the great potential of integrating the bottom-up and top-down SPPs for generating more accurate precipitation estimates. We believe the findings of the study will not only provide useful information to the data users to select an appropriate SPP, but also to the data producers to further enhance their precipitation retrieval algorithms.

Declaration of Competing Interest

The authors declare that they have no known competing financial interests or personal relationships that could have appeared to influence the work reported in this paper.

Acknowledgements

This study was supported by the Strategic Priority Research Program of Chinese Academy of Sciences (XDA20100104 and XDA19040504), the National Natural Science Foundation of China (41901045 and 41471448), and the CAS “Light of West China” Program (29Y929661). The authors would like to thank the China Meteorological Data Services Center for providing ground-based precipitation observations. We also wish to express our gratitude to Prof. Luca Brocca for providing us with the data, and for many very helpful discussions. In addition, we acknowledge Prof. Yang Hong and Dr. Xi Li for providing the subregion map of China.

References

Bárdossy, A., Pegram, G., 2013. Interpolation of precipitation under topographic influence at different time scales. Water Resour. Res. 49 (8), 4545–4565. https://doi.org/

10.1002/wrcr.20307.
Bharti, V., Singh, C., 2015. Evaluation of error in TRMM 3B42V7 precipitation estimates over the Himalayan region. J. Geophys. Res. Atmos. 120 (24), 12458–12473. https://doi.org/10.1002/2015JD023779.
Brocca, L., Ciabatta, L., Massari, C., et al., 2014. Soil as a natural rain gauge: Estimating global rainfall from satellite soil moisture data. J. Geophys. Res. Atmos. 119 (9), 5128–5141. https://doi.org/10.1002/2014JD021489.
Brocca, L., Filippucci, P., Hahn, S., et al., 2019. SM2RAIN–ASCAT (2007–2018): global daily satellite rainfall data from ASCAT soil moisture observations. Earth Syst. Sci. Data 11 (4), 1583–1601. https://doi.org/10.5194/essd-11-1583-2019.
Brocca, L., Moramarco, T., Melone, F., et al., 2013. A new method for rainfall estimation through soil moisture observations. Geophys. Res. Lett. 40 (5), 853–858. https://doi.org/10.1002/grl.50173.
Brocca, L., Pellarin, T., Crow, W.T., et al., 2016. Rainfall estimation by inverting SMOS soil moisture estimates: A comparison of different methods over Australia. J. Geophys. Res. Atmos. 121 (20), 12062–12079. https://doi.org/10.1002/2016JD025382.
Brunetti, M.T., Melillo, M., Peruccacci, S., et al., 2018. How far are we from the use of satellite rainfall products in landslide forecasting? Remote Sens. Environ. 210, 65–75. https://doi.org/10.1016/j.rse.2018.03.016.
Chen, F., Li, X., 2016. Evaluation of IMERG and TRMM 3B43 Monthly Precipitation Products over Mainland China. Remote Sensing 8 (6), 472. https://doi.org/10.3390/rs8060472.
Chen, S., Hong, Y., Cao, Q., et al., 2013. Similarity and difference of the two successive V6 and V7 TRMM multisatellite precipitation analysis performance over China. J. Geophys. Res. Atmos. 118 (23), 13060–13074. https://doi.org/10.1002/2013JD019964.
Chen, W.-T., Wu, C.-M., Ma, H.-Y., 2019. Evaluating the Bias of South China Sea Summer Monsoon Precipitation Associated with Fast Physical Processes Using a Climate Model Hindcast Approach. J. Clim. 32 (14), 4491–4507. https://doi.org/10.1175/JCLI-D-18-0660.1.
Chiaravalloti, F., Brocca, L., Procopio, A., et al., 2018. Assessment of GPM and SM2RAIN-ASCAT rainfall products over complex terrain in southern Italy. Atmos. Res. 206, 64–74. https://doi.org/10.1016/j.atmosres.2018.02.019.
Ciabatta, L., Brocca, L., Massari, C., et al., 2015. Integration of Satellite Soil Moisture and Rainfall Observations over the Italian Territory. J. Hydrometeorol. 16 (3), 1341–1355. https://doi.org/10.1175/JHM-D-14-0108.1.
Ciabatta, L., Marra, A.C., Panegrossi, G., et al., 2017. Daily precipitation estimation through different microwave sensors: Verification study over Italy. J. Hydrol. 545, 436–450. https://doi.org/10.1016/j.jhydrol.2016.12.057.
Ciabatta, L., Massari, C., Brocca, L., et al., 2018. SM2RAIN-CCI: a new global long-term rainfall data set derived from ESA CCI soil moisture. Earth Syst. Sci. Data 10 (1), 267–280. https://doi.org/10.5194/essd-10-267-2018.
Dezfuli, A.K., Ichoku, C.M., Huffman, G.J., et al., 2017. Validation of IMERG Precipitation in Africa. J. Hydrometeorol. 18 (10), 2817–2825. https://doi.org/10.1175/JHM-D-17-0139.1.
Dorigo, W., Wagner, W., Albergel, C., et al., 2017. ESA CCI Soil Moisture for improved Earth system understanding: State-of-the art and future directions. Remote Sens. Environ. 203, 185–215. https://doi.org/10.1016/j.rse.2017.07.001.
Duan, Q., Ajami, N.K., Gao, X., et al., 2007. Multi-model ensemble hydrologic prediction using Bayesian model averaging. Adv. Water Resour. 30 (5), 1371–1386. https://doi.org/10.1016/j.advwatres.2006.11.014.
Ebrahimi, S., Chen, C., Chen, Q., et al., 2017. Effects of temporal scales and space mismatches on the TRMM 3B42 v7 precipitation product in a remote mountainous area. Hydrol. Process. 31 (24), 4315–4327. https://doi.org/10.1002/hyp.11357.
Hsu, K.-L., Gao, X., Sorooshian, S., et al., 1997. Precipitation Estimation from Remotely Sensed Information Using Artificial Neural Networks. J. Appl. Meteorol. 36 (9), 1176–1190. https://doi.org/10.1175/1520-0450(1997) 036<1176:PEFRSI>2.0.CO;2.
Hu, Z., Zhou, Q., Chen, X., et al., 2018. Evaluation of three global gridded precipitation data sets in central Asia based on rain gauge observations. Int. J. Climatol. 38 (9), 3475–3493. https://doi.org/10.1002/joc.5510.
Huang, A., Zhao, Y., Zhou, Y., et al., 2016. Evaluation of multisatellite precipitation products by use of ground-based data over China. J. Geophys. Res. Atmos. 121 (18), 10654–10675. https://doi.org/10.1002/2016JD025456.
Huffman, G., Bolvin, D., Braithwaite, D. et al., 2014. Integrated Multi-satellitE Retrievals for GPM (IMERG), version 4.4. NASA's Precipitation Processing Center, accessed 31 March, 2015, ftp://arthurhou.pps.eosdis.nasa.gov/gpmdata/.
Huffman, G.J., Bolvin, D.T., Nelkin, E.J. et al., 2019. Integrated Multi-satellitE Retrievals for GPM (IMERG) Technical Documentation, https://docserver.gesdisc.eosdis.nasa.gov/public/project/GPM/IMERG_doc.06.pdf.
Huffman, G.J., Bolvin, D.T., Nelkin, E.J., et al., 2007. The TRMM Multisatellite Precipitation Analysis (TMPA): Quasi-Global, Multiyear, Combined-Sensor Precipitation Estimates at Fine Scales. J. Hydrometeorol. 8 (1), 38–55. https://doi.org/10.1175/JHM560.1.
Hui-Mean, F., Yusop, Z., Yusof, F., 2018. Drought analysis and water resource availability using standardised precipitation evapotranspiration index. Atmos. Res. 201, 102–115. https://doi.org/10.1016/j.atmosres.2017.10.014.
Jiang, L., Bauer-Gottwein, P., 2019. How do GPM IMERG precipitation estimates perform as hydrological model forcing? Evaluation for 300 catchments across Mainland China. J. Hydrol. 572, 486–500. https://doi.org/10.1016/j.jhydrol.2019.03.042.
Joyce, R.J., Janowiak, J.E., Arkin, P.A., et al., 2004. CMORPH: A Method that Produces Global Precipitation Estimates from Passive Microwave and Infrared Data at High Spatial and Temporal Resolution. J. Hydrometeorol. 5 (3), 487–503. https://doi.org/10.1175/1525-7541(2004) 005<0487:CAMTPG>2.0.CO;2.
Kucera, P.A., Ebert, E.E., Turk, F.J., et al., 2012. Precipitation from Space: Advancing Earth System Science. Bull. Am. Meteorol. Soc. 94 (3), 365–375. https://doi.org/10.1175/BAMS-D-11-00171.1.
Li, R., Wang, K., Qi, D., 2018. Validating the Integrated Multisatellite Retrievals for Global Precipitation Measurement in Terms of Diurnal Variability With Hourly Gauge Observations Collected at 50,000 Stations in China. J. Geophys. Res.: Atmos. 123 (18), 10423–10442. https://doi.org/10.1029/2018JD028991.
Li, Z., Yang, D., Hong, Y., 2013. Multi-scale evaluation of high-resolution multi-sensor blended global precipitation products over the Yangtze River. J. Hydrol. 500, 157–169. https://doi.org/10.1016/j.jhydrol.2013.07.023.
Lima, G.N.d., Lombardo, M.A., Magaña, V., 2018. Urban water supply and the changes in the precipitation patterns in the metropolitan area of São Paulo – Brazil. Appl. Geogr. 94: 223-229. doi:10.1016/j.apgeog.2018.03.010.
Ma, Y., Hong, Y., Chen, Y., et al., 2018. Performance of Optimally Merged Multisatellite Precipitation Products Using the Dynamic Bayesian Model Averaging Scheme Over the Tibetan Plateau. J. Geophys. Res. Atmos. 123 (2), 814–834. https://doi.org/10.1002/2017JD026648.
Massari, C., Brocca, L., Moramarco, T., et al., 2014. Potential of soil moisture observations in flood modelling: Estimating initial conditions and correcting rainfall. Adv. Water Resour. 74, 44–53. https://doi.org/10.1016/j.advwatres.2014.08.004.
Mastrantonas, N., Bhattacharya, B., Shibuo, Y., et al., 2019. Evaluating the Benefits of Merging Near-Real-Time Satellite Precipitation Products: A Case Study in the Kinu Basin Region, Japan. J. Hydrometeorol. 20 (6), 1213–1233. https://doi.org/10.1175/JHM-D-18-0190.1.
Omranian, E., Sharif, H., Tavakoly, A., 2018. How Well Can Global Precipitation Measurement (GPM) Capture Hurricanes? Case Study: Hurricane Harvey. Remote Sensing 10 (7), 1150. https://doi.org/10.3390/rs10071150.
Palomino-Ángel, S., Anaya-Acevedo, J.A., Botero, B.A., 2019. Evaluation of 3B42V7 and IMERG daily-precipitation products for a very high-precipitation region in northwestern South America. Atmos. Res. 217, 37–48. https://doi.org/10.1016/j.atmosres.2018.10.012.
Paredes-Trejo, F., Barbosa, H., Dos Santos, C.A.C., 2019. Evaluation of the Performance of SM2RAIN-Derived Rainfall Products over Brazil. Remote Sensing 11 (9), 1113. https://doi.org/10.3390/rs11091113.
Paredes-Trejo, F., Barbosa, H., Rossato Spatafora, L., 2018. Assessment of SM2RAIN-Derived and State-of-the-Art Satellite Rainfall Products over Northeastern Brazil. Remote Sensing 10 (7), 1093. https://doi.org/10.3390/rs10071093.
Prakash, S., 2019. Performance assessment of CHIRPS, MSWEP, SM2RAIN-CCI, and TMPA precipitation products across India. J. Hydrol. 571, 50–59. https://doi.org/10.1016/j.jhydrol.2019.01.036.
Qing, P., Cai, C., Wu, Z., 2018. Comparison of the the double tipping bucket and weighing rain gauges (in Chinese). Guangdong Meteorology 40 (2), 69–72.
Rahman, U.K., Shang, S., Shahid, M., et al., 2019a. Performance Assessment of SM2RAIN-CCI and SM2RAIN-ASCAT Precipitation Products over Pakistan. Remote Sensing 11(17). doi:10.3390/rs11172040.
Rahman, U.K., Shang, S., Shahid, M., et al., 2019b. Performance Assessment of SM2RAIN-CCI and SM2RAIN-ASCAT Precipitation Products over Pakistan. Remote Sensing 11 (17), 2040. https://doi.org/10.3390/rs11172040.
Rozante, J., Vila, D., Barboza Chiquetto, J., et al., 2018. Evaluation of TRMM/GPM Blended Daily Products over Brazil. Remote Sensing 10 (6), 882. https://doi.org/10.3390/rs10060882.
Shen, Y., Xiong, A., Hong, Y., et al., 2014. Uncertainty analysis of five satellite-based precipitation products and evaluation of three optimally merged multi-algorithm products over the Tibetan Plateau. Int. J. Remote Sens. 35 (19), 6843. https://doi.org/10.1080/01431161.2014.960612.
Shen, Y., Xiong, A., Wang, Y., et al., 2010. Performance of high-resolution satellite precipitation products over China. J. Geophys. Res. 115, D02114. https://doi.org/10.1029/2009JD012097.
Sorooshian, S., Hsu, K.-L., Gao, X., et al., 2000. Evaluation of PERSIANN System Satellite-Based Estimates of Tropical Rainfall. Bull. Am. Meteorol. Soc. 81 (9), 2035–2046. https://doi.org/10.1175/1520-0477(2000) 081<2035:EOPSSE>2.3.CO;2.
Supit, I., van Diepen, C.A., de Wit, A.J.W., et al., 2012. Assessing climate change effects on European crop yields using the Crop Growth Monitoring System and a weather generator. Agric. For. Meteorol. 164, 96–111. https://doi.org/10.1016/j.agrformet.2012.05.005.
Tang, G., Behrangi, A., Long, D., et al., 2018. Accounting for spatiotemporal errors of gauges: A critical step to evaluate gridded precipitation products. J. Hydrol. 559, 294–306. https://doi.org/10.1016/j.jhydrol.2018.02.057.
Tang, G., Ma, Y., Long, D., et al., 2016. Evaluation of GPM Day-1 IMERG and TMPA Version-7 legacy products over Mainland China at multiple spatiotemporal scales. J. Hydrol. 533, 152–167. https://doi.org/10.1016/j.jhydrol.2015.12.008.
Tarpanelli, A., Massari, C., Ciabatta, L., et al., 2017. Exploiting a constellation of satellite soil moisture sensors for accurate rainfall estimation. Adv. Water Resour. 108, 249–255. https://doi.org/10.1016/j.advwatres.2017.08.010.
Tian, F., Hou, S., Yang, L., et al., 2018. How Does the Evaluation of the GPM IMERG Rainfall Product Depend on Gauge Density and Rainfall Intensity? J. Hydrometeorol. 19 (2), 339–349. https://doi.org/10.1175/JHM-D-17-0161.1.
Tian, Y., Zheng, Y., Wu, B., et al., 2015. Modeling surface water-groundwater interaction in arid and semi-arid regions with intensive agriculture. Environ. Modell. Software 63, 170–184. https://doi.org/10.1016/j.envsoft.2014.10.011.
Wagner, W., Hahn, S., Kidd, R., et al., 2012. The ASCAT Soil Moisture Product: Specifications, Validation, Results, and Emerging Applications, submitted to. Meteorol. Z. 22 (1), 5–33.
Wang, X., Ding, Y., Zhao, C., et al., 2019a. Similarities and improvements of GPM IMERG upon TRMM 3B42 precipitation product under complex topographic and climatic conditions over Hexi region, Northeastern Tibetan Plateau. Atmos. Res. 218, 347–363. https://doi.org/10.1016/j.atmosres.2018.12.011.

Wang, Y., 2017. The connection method of the tipping bucket and weighing rain gauges (in. Chinese). Modern Agricultural Technology(3), 210–212.
Wang, Z., Ye, A., Wang, L., et al., 2019b. Spatial and temporal characteristics of reference evapotranspiration and its climatic driving factors over China from 1979–2015. Agric. Water Manag. 213, 1096–1108. https://doi.org/10.1016/j.agwat.2018.12.006.
Wei, G., Lü, H., Crow, T., W, et al., 2018. Evaluation of Satellite-Based Precipitation Products from IMERG V04A and V03D, CMORPH and TMPA with Gauged Rainfall in Three Climatologic Zones in China. Remote Sensing 10 (2), 30. https://doi.org/10.3390/rs10010030.
Xu, R., Tian, F., Yang, L., et al., 2017. Ground validation of GPM IMERG and TRMM 3B42V7 rainfall products over southern Tibetan Plateau based on a high-density rain gauge network. J. Geophys. Res. Atmos. 122 (2), 910–924. https://doi.org/10.1002/2016JD025418.
Ye, B., Yang, D., Ding, Y., et al., 2004. A Bias-Corrected Precipitation Climatology for China. J. Hydrometeorol. 5 (6), 1147–1160. https://doi.org/10.1175/JHM-366.1.
Yu, W., Nan, Z., Wang, Z., et al., 2015. An Effective Interpolation Method for MODIS Land Surface Temperature on the Qinghai-Tibet Plateau. IEEE J. Sel. Top. Appl. Earth Obs. Remote Sens. 8 (9), 4539–4550. https://doi.org/10.1109/JSTARS.2015.2464094.
Yuan, F., Wang, B., Shi, C., et al., 2018. Evaluation of hydrological utility of IMERG Final run V05 and TMPA 3B42V7 satellite precipitation products in the Yellow River source region, China. J. Hydrol. 567, 696–711. https://doi.org/10.1016/j.jhydrol.2018.06.045.
Yuan, F., Zhang, L., Soe, K., et al., 2019. Applications of TRMM- and GPM-Era Multiple-Satellite Precipitation Products for Flood Simulations at Sub-Daily Scales in a Sparsely Gauged Watershed in Myanmar. Remote Sensing 11 (2), 140. https://doi.org/10.3390/rs11020140.
Zhao, T., Yatagai, A., 2014. Evaluation of TRMM 3B42 product using a new gauge-based analysis of daily precipitation over China. Int. J. Climatol. 34 (8), 2749–2762. https://doi.org/10.1002/joc.3872.
Zhong, R., Chen, X., Lai, C., et al., 2019. Drought monitoring utility of satellite-based precipitation products across mainland China. J. Hydrol. 568, 343–359. https://doi.org/10.1016/j.jhydrol.2018.10.072.